Neyman Pearson Detection of K-Distributed Random Variables

J. Derek Tucker[a,b] and Mahmood R. Azimi-Sadjadi[b]

[a]Naval Surface Warfare Center, Panama City Division,
110 Vernon Ave Panama City, FL, USA 32407;
[b]Department of Electrical and Computer Engineering, Colorado State University,
1373 Campus Delivery Fort Collins, CO, USA 80523

ABSTRACT

In this paper a new detection method for sonar imagery is developed in $\mathcal{K}$-distributed background clutter. The equation for the log-likelihood is derived and compared to the corresponding counterparts derived for the Gaussian and Rayleigh assumptions. Test results of the proposed method on a data set of synthetic underwater sonar images is also presented. This database contains images with targets of different shapes inserted into backgrounds generated using a correlated $\mathcal{K}$-distributed model. Results illustrating the effectiveness of the $\mathcal{K}$-distributed detector are presented in terms of probability of detection, false alarm, and correct classification rates for various bottom clutter scenarios.

Keywords: $\mathcal{K}$-distributed clutter, non-Gaussian signal detection, sonar imagery, target detection and classification

1. INTRODUCTION

The problem of underwater object detection and classification in sonar imagery has attracted a substantial amount of attention.[1–6] This problem is complicated due to various factors such as variations in operating and environmental conditions, presence of spatially varying clutter, variations in target shapes, compositions and orientation. Moreover, bottom features such as coral reefs, sand formations, and vegetation may totally obscure a target or confuse the detection process. Consequently, a robust detection system should be able to quantify changes between the returns from the bottom and any target activity in sonar images, while at the same time extract useful features for subsequent classification. Thus, a robust system designed to mitigate false alarms in various clutter density scenarios will be desirable.

Considerable research has been devoted to the development of different detector and classification methodologies to detect and classify underwater objects from sonar imagery. Dobeck[1,2] utilized a nonlinear matched filter to identify mine-size regions that match the target template in a side-scan sonar image. For each detected region, several features were extracted based on the size, shape, and strength of the target template. A stepwise feature selection process was then used to determine the subset of features that maximizes the probability of detection and classification. A k-nearest neighbor and an optimal discrimination filter classifier were used to classify each feature vector and the decisions of the two classifiers were fused to generate the final decision. In,[3] a method was proposed that first median filters the sonar image to reduce the speckle noise present in the image. The image was then split into overlapping range segments where the pixels in each segment were adaptively thresholded. The threshold was determined from cumulative distribution function (CDF) formed from a training set. Geometric features were then extracted from contiguous target structure regions within the segment and classification of each region as target or non-target was done through a multi-level weighted scoring-based classification system. In,[7] the adaptive clutter filter detector in[8] was individually applied to three different sonar images varying in frequency and bandwidth. Final classification is done using an optimal set of features using

Approved for public release; distribution is unlimited
Further author information: (Send correspondence to Mr. J. Derek Tucker)
J. D. Tucker: E-mail: james.d.tucker@navy.mil, Telephone: 1 850 636 6090

a nonlinear log-likelihood ratio test where the decisions of the individual detector and classifier are fused. Recently in[5,6] we developed a new coherence-based detection framework for dual-sensor problem using Canonical Coordinate Analysis (CCA) that can be applied to the data collected using two disparate sonar systems. Using this method allows for the simultaneous detection and feature extraction of coherent target information among two sonar images.

The coherence-based detection method in[5,6] used the standard CCA method and this method inherently relies on the Gaussian assumption of both signal and noise. Due to this assumption, one is not able to accurately represent the bottom clutter and hence the performance gain is limited. This is due to the fact that recent studies on bottom clutter statistics reveal[9–12] that the distribution of the envelope of the matched filtered output is dependent on the frequency, grazing angle, range and roughness properties of the bottom. Rough surface measurements made using high resolution sonar have indicated[9] that the envelope amplitude distributions can be modeled by Rayleigh, log-normal, Weibull or other more complex distributions such as the $\mathcal{K}$-distribution.[11,12] This suggests that the underlying complex data is not Gaussian and that second-order moments will not be sufficient for detection and classification purposes, thus impairing the overall performance. This motivates our interest in a non-Gaussian background based detection method. In,[11,12] the authors used the $\mathcal{K}$-distribution to model textured background in sonar imagery. Model parameters are estimated from a set of textured sonar images using a nonlinear least-squares algorithm. The model was then validated against textures extracted from high-frequency synthetic aperture sonar (SAS) imagery background.

In this paper a new detection method for high-resolution sonar imagery is developed using optimal Neyman-Pearson detection[13] for $\mathcal{K}$-distributed background clutter. A new formulation of the log-likelihood ratio is developed for the $\mathcal{K}$-distribution and compared to those of the Gaussian and Rayleigh distributions. Our *detection hypothesis* in this non-Gaussian detection framework is that presence of objects in the sonar data leads to a change in the parameters of the $\mathcal{K}$-distribution comparing to that of the background clutter only. The data set used in this study was provided by the Naval Surface Warfare Center Panama City Division (NSWC PCD) in Panama City, FL. The data-set consists of synthetically generated sonar image snippets varying in target shape, background type, aspect angle, range, and signal-to-noise ratio (SNR).

This paper is organized as follows: Section 2 reviews and develops the pdf for the $\mathcal{K}$-distribution. Section 3 offers a brief review on standard signal detection theory. Section 4 develops the log-likelihood ratio for the $\mathcal{K}$-distribution and compares it to the log-likelihood ratios for the Rayleigh and Gaussian distributions. In Section 5, the results using the detectors developed in Section 4 on synthetically generating SAS imagery will be presented. Finally, conclusions and observations are offered in Section 6.

2. $\mathcal{K}$-DISTRIBUTION FOR MODELING BACKGROUND CLUTTER

The $\mathcal{K}$-distribution has been developed and motivated from the work in the distribution of radar echo's from the sea surface. In the past sonar backscatter from the sea bottom has been modeled as Rayleigh distributed as the envelope of the sonar return is assumed to be the square root of the sum from many independent complex Gaussian-distributed scatterers. However, this assumption fails when the nature of the clutter on the bottom is such that the number of scatterers is small and the Central Limit Theorem is invalid. In recent work, Ward[14] has modeled high-resolution radar scattering phenomena through the compound $\mathcal{K}$-distribution. In the compound $\mathcal{K}$-distribution the probability density function of the signal amplitude X originates from the product of two component densities: 1) a speckle component that is Rayleigh-distributed with square-root Gamma-distributed parameter Y, and 2) a square-root Gamma distribution with parameters related to the radar or sonar system resolution and environmental conditions. A brief review of the derivation of the $\mathcal{K}$-distribution beginning with the above assumptions of the compound distribution is provided below.

Assign $p_{X|Y}(x|y)$ the Rayleigh probability density function (pdf) with random parameter Y

$$p_{X|Y}(x|y) = \frac{x}{y^2} e^{\frac{-x^2}{2y^2}} u(x) \tag{1}$$

where $u(x)$ is the unit step function.

Assume $p_Z(z)$ is the Gamma pdf with parameters ν and b

$$p_Z(z) = \frac{b^\nu}{\Gamma(\nu)} z^{\nu-1} e^{-bz} u(z). \tag{2}$$

The square-root Gamma pdf is $p_Y(y) = 2y p_Z(y^2)$ thus the function form of the square-root Gamma pdf in terms of y is

$$p_Y(y) = \frac{2yb^\nu}{\Gamma(\nu)} y^{2\nu-2} e^{-by^2} u(y). \tag{3}$$

Let $p_X(x)$ represent the pdf of the signal envelope. The compound representation follow from the use of Bayes rule and marginalization over variable y,

$$p_X(x) = \int_{-\infty}^{\infty} p_{X|Y}(x|y) p_Y(y)\, dy = \frac{xb^\nu}{\Gamma(\nu)} \int_0^\infty y^{-2} y^{2\nu-2} e^{-\frac{x^2}{2y^2} - by^2} 2y\, dy. \tag{4}$$

Define $C_1 = \frac{xb^\nu}{\Gamma(\nu)}$ and use integration by parts, we get

$$\begin{aligned} p_X(x) &= C_1 \int_0^\infty u^{\nu-2} e^{-\frac{x^2}{2u} - bu}\, du \\ &= C_1 \int_0^\infty u^{\gamma-1} e^{-\frac{x^2}{2u} - bu}\, du \end{aligned} \tag{5}$$

where $\gamma = \nu - 1$. From[15] we have $\int_0^\infty u^{\gamma-1} e^{-\frac{\beta}{u} - \rho u}\, du = 2\left(\frac{\beta}{p}\right)^{\frac{\gamma}{2}} K_\gamma(2\sqrt{\beta\rho})$, where $K_\gamma(\cdot)$ is the modified Bessel function of the second kind. By setting $\beta = \frac{x^2}{2}$ and $\rho = b$ we can rewrite $p_X(x)$ as

$$p_X(x) = 2C_1 \left(\frac{x^2}{2b}\right)^{\frac{\gamma}{2}} K_\gamma\left(2x\sqrt{\frac{b}{2}}\right). \tag{6}$$

Substituting $\nu - 1 = \gamma$ and $C_1 = \frac{xb^\nu}{\Gamma(\nu)}$ and $\alpha = \sqrt{2b}$ we get

$$p_X(x) = \frac{2\alpha}{\Gamma(\nu)} \left(\frac{\alpha x}{2}\right)^\nu K_{\nu-1}(\alpha x) u(x), \tag{7}$$

which is the familiar pdf of the $\mathcal{K}$-distribution[14,16,17] with shape parameter ν and scale parameter α. An example of the pdf of the $\mathcal{K}$-distribution is presented in Figure 1. There are two examples presented here, one for background only ($\alpha = 53$, $\nu = 0.1$) and another for target plus background ($\alpha = 80$, $\nu = -0.3$), where for both cases the parameters were estimated from data with the same background. This figure confirms our detection hypothesis made previously.

3. A BRIEF REVIEW OF BAYESIAN DETECTION THEORY

In this section we review standard Bayesian detection theory. Consider the classical detection problem of choosing between two hypotheses[13] where each hypothesis relates to a point in the N-dimensional observation space. In other words, if $\mathbf{x} = [x_1, x_2, \cdots, x_N]^H$, is an observation vector in this space we would like to test between H_1 hypothesis (true) and H_0 hypothesis (null) for this observation vector. Clearly, each time we conduct the test there are four possible outcomes. Those are: (1) H_0 is true and we choose H_0, (2) H_0 is true and we choose H_1, (3) H_1 is true and we choose H_1, and (4) H_1 is true but we choose H_0. The first and third outcomes lead to correct decisions while the second and fourth outcomes lead to erroneous decisions. The Bayes test is based on two assumptions. First, the two hypotheses, H_0 and H_1, correspond to two possible prior probabilities, P_0 and P_1, respectively. These probabilities represent the prior observer's information about the hypotheses before the detection is conducted. The second assumption is that there is a cost associated with each of the four courses of action described above. These costs will be denoted by, C_{00}, C_{10}, C_{11}, and C_{01}, for outcomes 1-4, respectively.

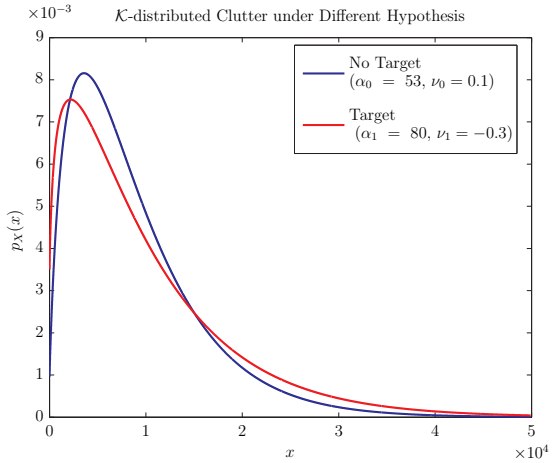

Figure 1: Example $\mathcal{K}$-distributed Clutter With and Without a Target.

Where C_{ij} represents the cost when hypothesis i is true and j is chosen, $i, j = 0, 1$. It will be assumed that the cost of a wrong decision is higher than the cost of a correct decision, i.e. $C_{10} > C_{00}$ and $C_{01} > C_{11}$. The goal of the Bayes test is to design a decision rule so that on the average cost of a decision will be as small as possible, which subsequently leads to the smallest Bayesian risk when making the decision. If we denote the expected value of the cost as the risk $\mathcal{R}$, we can then write $\mathcal{R}$ as,[13]

$$\mathcal{R} = C_{00}P_0P(H_0|H_0) + C_{10}P_0P(H_1|H_0) + C_{11}P_1P(H_1|H_1) + C_{01}P_1P(H_0|H_1) \tag{8}$$

where $P(H_j|H_i)$ $i, j \in [0, 1]$ is the probability that we choose H_j given that the true hypothesis is H_i.

Since the decision rule is binary either H_0 and H_1, we can view the rules as a division in the observation space into two parts A_0 and A_1. In other words, if the observation is found in the region A_0 the hypothesis H_0 is declared true and if the observation is found in the region A_1 the hypothesis H_1 is declared true. By viewing the problem in this manner we can now express the risk in terms of the decision regions and probabilities as,

$$\begin{aligned}\mathcal{R} &= C_{00}P_0\int_{A_0} p_{\mathbf{X}|H_0}(\mathbf{x}|H_0)\,d\mathbf{x} + C_{10}P_0\int_{A_1} p_{\mathbf{X}|H_0}(\mathbf{x}|H_0)\,d\mathbf{x} + C_{11}P_1\int_{A_1} p_{\mathbf{X}|H_1}(\mathbf{x}|H_1)\,d\mathbf{x} \\ &\quad + C_{01}P_1\int_{A_0} p_{\mathbf{X}|H_1}(\mathbf{x}|H_1)\,d\mathbf{x}.\end{aligned} \tag{9}$$

To find the decision rule, the decision regions are determined such that the risk in (9) is minimized. Because each element of $\mathbf{x}$ must be assigned to either the A_0 or A_1 in the observation space A, we can say that $A = A_0 \cup A_1$ and $A_0 \cap A_1 = \emptyset$. Now, (9) can be rewritten as[13]

$$\begin{aligned}\mathcal{R} &= P_0C_{00}\int_{A_0} p_{\mathbf{X}|H_0}(\mathbf{x}|H_0)\,d\mathbf{x} + P_0C_{10}\int_{A-A_0} p_{\mathbf{X}|H_0}(\mathbf{x}|H_0)\,d\mathbf{x} \\ &\quad + P_1C_{01}\int_{A_0} p_{\mathbf{X}|H_1}(\mathbf{x}|H_1)\,d\mathbf{x} + P_1C_{11}\int_{A-A_0} p_{\mathbf{X}|H_1}(\mathbf{x}|H_1)\,d\mathbf{x}.\end{aligned} \tag{10}$$

We can separate the integrals and rewrite (10) as,

$$\begin{aligned}\mathcal{R} &= P_0C_{00}\int_{A_0} p_{\mathbf{X}|H_0}(\mathbf{x}|H_0)\,d\mathbf{x} + P_0C_{10}\int_{A} p_{\mathbf{X}|H_0}(\mathbf{x}|H_0)\,d\mathbf{x} - P_0C_{10}\int_{A_0} p_{\mathbf{X}|H_0}(\mathbf{x}|H_0)\,d\mathbf{x} \\ &\quad + P_1C_{01}\int_{A_0} p_{\mathbf{X}|H_1}(\mathbf{x}|H_1)\,d\mathbf{x} + P_1C_{11}\int_{A} p_{\mathbf{X}|H_1}(\mathbf{x}|H_1)\,d\mathbf{x} - P_1C_{11}\int_{A_0} p_{\mathbf{X}|H_1}(\mathbf{x}|H_1)\,d\mathbf{x}\end{aligned} \tag{11}$$

If we use $\int_A p_{\mathbf{X}|H_0}(\mathbf{x}|H_0)\,d\mathbf{x} = \int_A p_{\mathbf{X}|H_1}(\mathbf{x}|H_1)\,d\mathbf{x} = 1$, then (11) can be reduced to,

$$\mathcal{R} = P_0C_{10} + P_1C_{11} + \int_{A_0}\left[P_1(C_{01} - C_{11})p_{\mathbf{X}|H_1}(\mathbf{x}|H_1) - P_0(C_{10} - C_{00})p_{\mathbf{X}|H_0}(\mathbf{x}|H_0)\right]\,d\mathbf{x} \tag{12}$$

The first two terms in (12) represent the fixed cost and the integral represents the cost controlled by the points in the observation space, A that are assigned to A_0. Basically, the points in A for which the first term in the integral is larger than the second term are assigned to A_1, whereas the points in which the second term is larger than the first term are assigned to A_0. Any points in which the terms are equal have no effect on the cost and can be arbitrarily assigned to any region (we assume that these points are assigned to A_1). We can, therefore, define the decision region in the observation space by

$$P_1(C_{01} - C_{11})p_{\mathbf{X}|H_1}(\mathbf{x}|H_1) \geq P_0(C_{10} - C_{00})p_{\mathbf{X}|H_0}(\mathbf{x}|H_0). \tag{13}$$

which can alternatively be rewritten as

$$\frac{p_{\mathbf{X}|H_1}(\mathbf{x}|H_1)}{p_{\mathbf{X}|H_0}(\mathbf{x}|H_0)} \underset{H_0}{\overset{H_1}{\gtrless}} \frac{P_0(C_{10} - C_{00})}{P_1(C_{01} - C_{11})}. \tag{14}$$

The quantity on the left is called the *likelihood ratio* and will be denoted throughout the rest of this paper by

$$l(\mathbf{x}) \triangleq \frac{p_{\mathbf{X}|H_1}(\mathbf{x}|H_1)}{p_{\mathbf{X}|H_0}(\mathbf{x}|H_0)}. \tag{15}$$

The relationship on the right is the threshold of the test and will be denoted by η. Thus, Bayes criterion simply leads to a likelihood ratio test, given by

$$l(\mathbf{x}) \underset{H_0}{\overset{H_1}{\gtrless}} \eta. \tag{16}$$

3.1 Neyman-Pearson Detection

In many practical detection situations it is difficult to assign realistic costs and prior probabilities. This is especially apparent for sonar imagery target detection due to the variations in target compositions and background clutter. To overcome this, a simple alternative is to use probabilities, P_{FA}, i.e. false alarm probability and, P_D, which is the probability of detection. This leads to the Neyman-Pearson criterion[13,18] which designs a test to maximize P_D while making P_{FA} as small as possible. The criterion constrains $P_{FA} = a' \leq a$ and designs a test that maximizes the probability of detection under this constraint.[13] The solution to this constrained optimization problem is found by using Lagrange multipliers, i.e., we can construct a function F,

$$F = P_D + \lambda[P_{FA} - a']. \tag{17}$$

Here by maximizing F we will maximize P_D. For ease in the rest of the derivation we will convert this to a minimization problem where the objective is to minimize the probability of a miss-detection, P_M which gives $F = P_M + \lambda[P_{FA} - a']$. We can then rewrite F in terms of the conditional probabilities as[13]

$$F = \int_{A_0} p_{\mathbf{X}|H_1}(\mathbf{x}|H_1)\, d\mathbf{x} + \lambda \left[\int_{A_1} p_{\mathbf{X}|H_0}(\mathbf{x}|H_0)\, d\mathbf{x} - a' \right]. \tag{18}$$

Clearly (18) is minimized when $P_{FA} = a'$, thus minimizing P_M for the non-trivial case when $\lambda \neq 0$. Using $A_0 = A - A_1$, we can then rewrite F as

$$F = \lambda(1 - a') + \int_{A_0} \left[p_{\mathbf{X}|H_1}(\mathbf{x}|H_1) - \lambda p_{\mathbf{X}|H_0}(\mathbf{x}|H_0) \right] d\mathbf{x} \tag{19}$$

For any positive value of λ a likelihood ratio test will minimize F.[13] This follows directly because by minimizing F we assign a point in $\mathbf{x}$ to A_1 when the integral is positive or assign the point to A_0 when the integral is negative. Therefore, we can write

$$l(\mathbf{x}) = \frac{p_{\mathbf{X}|H_1}(\mathbf{x}|H_1)}{p_{\mathbf{X}|H_0}(\mathbf{x}|H_0)} \underset{H_0}{\overset{H_1}{\gtrless}} \lambda. \tag{20}$$

Although this is similar to (16), the threshold in (20) does no-longer rely on the *prior* probabilities and the assigned costs.

4. DETECTION IN $\mathcal{K}$-DISTRIBUTED DATA

If we now view this detection problem in terms $\mathcal{K}$-distributed sonar clutter, the decision between two hypotheses is now either background only (H_0) or signal plus background (H_1). Assume we have a scalar observation $x \in \mathbb{R}$, which is a $\mathcal{K}$-distributed random variable with scale parameter α and shape parameter ν. We wish to test the hypothesis $H_0 : [\alpha, \nu] = [\alpha_0, \nu_0]$, i.e. background alone versus $H_1 : [\alpha, \nu] = [\alpha_1, \nu_1]$, i.e signal plus background, where the shape and scale of the $\mathcal{K}$-distribution change with the presence of the target (see Figure 1).

Therefore using (20) the likelihood ratio under this detection model becomes

$$l(x) = \frac{\frac{2\alpha_1}{\Gamma(\nu_1)}\left(\frac{\alpha_1 x}{2}\right)^{\nu_1} K_{\nu_1-1}(\alpha_1 x)}{\frac{2\alpha_0}{\Gamma(\nu_0)}\left(\frac{\alpha_0 x}{2}\right)^{\nu_0} K_{\nu_0-1}(\alpha_0 x)}. \tag{21}$$

The modified Bessel function of the second kind can be well approximated by[19]

$$K_n(y) \approx \frac{e^{-y}}{\sqrt{\frac{2}{\pi}y}} \tag{22}$$

if $y \gg n$.

This assumption is valid[11,12] for sonar imagery as the shape parameter minus 1 $(\nu - 1)$ is much smaller than the pixel intensity times the scale (αx). Therefore, if we replace the Bessel function in (21) by this approximated version in (22) the likelihood can be rewritten as

$$l(x) = \frac{\frac{2\alpha_1}{\Gamma(\nu_1)}\left(\frac{\alpha_1 x}{2}\right)^{\nu_1} \frac{e^{-\alpha_1 x}}{\sqrt{\frac{2}{\pi}\alpha_1 x}}}{\frac{2\alpha_0}{\Gamma(\nu_0)}\left(\frac{\alpha_0 x}{2}\right)^{\nu_0} \frac{e^{-\alpha_0 x}}{\sqrt{\frac{2}{\pi}\alpha_0 x}}}. \tag{23}$$

By taking the natural logarithm of both sides we form the log-likelihood ratio,

$$\ln(l(x)) = \ln\left(\frac{2\alpha_1}{\Gamma(\nu_1)}\right) + \nu_1 \ln\left(\frac{\alpha_1 x}{2}\right) + \ln\left(\frac{e^{-\alpha_1 x}}{\sqrt{\frac{2}{\pi}\alpha_1 x}}\right) - \ln\left(\frac{2\alpha_0}{\Gamma(\nu_0)}\right) - \nu_0 \ln\left(\frac{\alpha_0 x}{2}\right) - \ln\left(\frac{e^{-\alpha_0 x}}{\sqrt{\frac{2}{\pi}\alpha_0 x}}\right). \tag{24}$$

By rearranging terms and dropping the constants that do not depend on the observation x, we get the following log-likelihood ratio

$$\ln(l(x)) = \nu_1 \ln(x) + (\alpha_0 - \alpha_1)x - \ln\left(\sqrt{\frac{2}{\pi}\alpha_1 x}\right) - \nu_0 \ln(x) + \ln\left(\sqrt{\frac{2}{\pi}\alpha_0 x}\right). \tag{25}$$

Again if we simplify and drop the constants we get the final log-likelihood ratio $(\Lambda(x))$, for $\mathcal{K}$-distributed random variables

$$\Lambda(x) = (\nu_1 - \nu_0)\ln(x) + (\alpha_0 - \alpha_1)x. \tag{26}$$

4.1 Comparison to Other Distributions

In order to make a complete study of the developed detector for $\mathcal{K}$-distributed data we develop in the following sections the log-likelihood ratios for Rayleigh and Gaussian distributed data.

4.1.1 Rayleigh

Now, let us view this detection problem in Rayleigh distributed sonar data with same hypothesis as in the previous section. Assume we have an observation $x \in \mathbb{R}$, which is Rayleigh distributed with parameter σ. We wish to test the hypothesis $H_0 : \sigma = \sigma_0$, i.e. background alone versus $H_1 : \sigma = \sigma_1$, i.e signal plus background, where the parameter of the Rayleigh distribution changes with the presence of a target.

Using the Rayleigh pdf, $f(x) = \frac{x}{\sigma^2} e^{-x^2/2\sigma^2}$ the likelihood ratio for this detection problem is

$$l(x) = \frac{\frac{x}{\sigma_1^2} e^{-x^2/2\sigma_1^2}}{\frac{x}{\sigma_0^2} e^{-x^2/2\sigma_0^2}}. \tag{27}$$

By taking the natural logarithm and using the properties of the log we can write the log-likelihood as

$$\ln(l(x)) = \ln(\sigma_0^2) - \ln(\sigma_1^2) + \left(\frac{1}{2\sigma_0^2} - \frac{1}{2\sigma_1^2}\right) x^2. \tag{28}$$

If we ignore the terms that are not x-dependent the final log-likelihood ratio for the Rayleigh assumption is

$$\Lambda(x) = \frac{\sigma_1^2 - \sigma_0^2}{2\sigma_0^2\sigma_1^2} x^2. \tag{29}$$

4.1.2 Gaussian

Now, let us view this detection problem in Gaussian distributed sonar data with same hypothesis as in the previous section. Assume we have an observation $x \in \mathbb{R}$, which is Gaussian distributed with zero mean and variance σ. We wish to test the hypothesis $H_0 : \sigma = \sigma_0$, i.e. background alone versus $H_1 : \sigma = \sigma_1$, i.e signal plus background, where the variance of the Gaussian distribution changes with the presence of a target.

Using the Gaussian pdf, $f(x) = \frac{1}{\sigma\sqrt{2\pi}} e^{-x^2/2\sigma^2}$ the likelihood ratio for this detection problem is

$$l(x) = \frac{\frac{1}{\sigma_1\sqrt{2\pi}} e^{-x^2/2\sigma_1^2}}{\frac{1}{\sigma_0\sqrt{2\pi}} e^{-x^2/2\sigma_0^2}}. \tag{30}$$

By taking the natural logarithm and using the properties of the log we can write the log-likelihood as

$$\ln(l(x)) = \ln\left(\frac{1}{\sigma_1\sqrt{2\pi}}\right) + \frac{-x^2}{2\sigma_1^2} - \ln\left(\frac{1}{\sigma_0\sqrt{2\pi}}\right) + \frac{x^2}{2\sigma_0^2}. \tag{31}$$

If we ignore the terms that are not x-dependent the final log-likelihood ratio for the Gaussian assumption is

$$\Lambda(x) = \left(\sigma_0^{-2} - \sigma_1^{-2}\right) x^2. \tag{32}$$

5. SIMULATION RESULTS

An experiment was conducted to show the performance of the $\mathcal{K}$-distributed detector versus the Rayleigh and Gaussian cases for sonar imagery data. Specifically we want to show that $\mathcal{K}$-distributed detector performs better of the Gaussian and Rayleigh assumptions are made, which most current SAS detection methods use and have a higher performance at a much lower false alarm rate. Moreover, we would like to study the sensitivity of the $\mathcal{K}$-distributed detector to different SNR, ν values (clutter density), and targets types.

A synthetic sonar image database generated using the method described in[11,12] was used for this study. Under H_0 the image is pure $\mathcal{K}$-distributed background with a corresponding shape and scale factor. The signal is a synthetically generated target inserted into the $\mathcal{K}$-distributed background. Therefore, under H_1 we have target plus background and both ν and α will change (see Figure 1). The image background was generated for three different shape parameters, specifically $\nu = -0.5, 0.5$, and 2. The target plus background was generated from namely three different target shapes a cylinder, cone, and sphere that are generated at 15 different rotations and for each rotation 5 different ranges. The SNR was changed by altering the target strength with respect to the mean background value. From these variable parameters a data set consisting of 1200 target images and 1200 background images was generated.

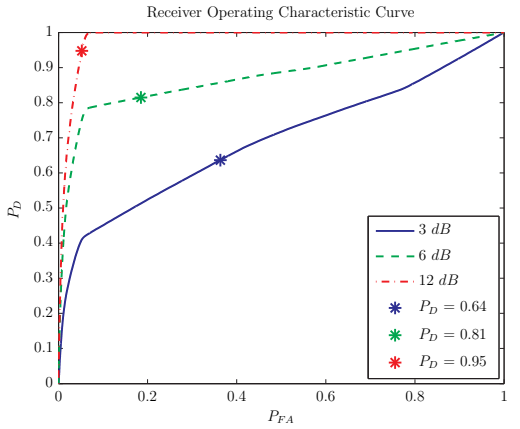

(a) K-Distribution

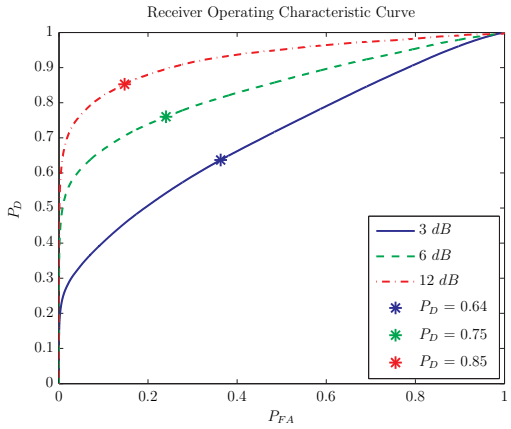

(b) Rayleigh Distribution

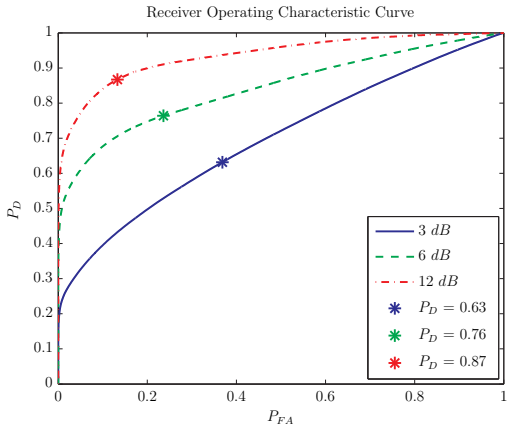

(c) Gaussian Distribution

Figure 2: Receiver Operating Characteristic Curves for Different Statistical Distribution Assumptions for Different SNR.

5.1 Performance Under Different SNR Calculations

For each value of ν in the database the detector is trained by estimating ν_0 and α_0 from 30 H_0 snippets and ν_1 and α_1 from 30 H_1 snippets. For the detection process, an image snippet is taken and for each pixel the log-likelihood is calculated using (26). The log-likelihood value is then compared against the detection threshold either a background pixel or target pixel is declared. The threshold is calculated from the 60 training samples described above by applying them to the trained detector. From the log-likelihood values receiver operating characteristic (ROC) curves were generated for each SNR in the dataset, specifically for 3, 6, and 12 dB. Figure 2a presents the ROC curves for the $\mathcal{K}$-distribution detector for 3, 6, and 12 dB with the knee points (where $P_D + P_{FA} = 1$), that are marked by a * and the corresponding P_D values.

For a complete comparison of the performance of the $\mathcal{K}$-distribution detector, ROC curves were also formed for both the Rayleigh and the Gaussian background cases. The ROC curves were generated the same way as the $\mathcal{K}$-distribution case except the the log-likelihood ratio was calculated using (29) for the Rayleigh and (32) for the Gaussian. Figures 2b and 2c present the ROC curves for these cases, respectively. As expected for all three distributions we see an increase in the performance of the detector as SNR increases. Specifically, for both 6 and 12 dB the $\mathcal{K}$-distributed detector has a much higher P_D for a lower P_{FA}, than those of the Rayleigh and Gaussian-based detectors. It is also interesting to note here that for a higher SNR the Gaussian detector

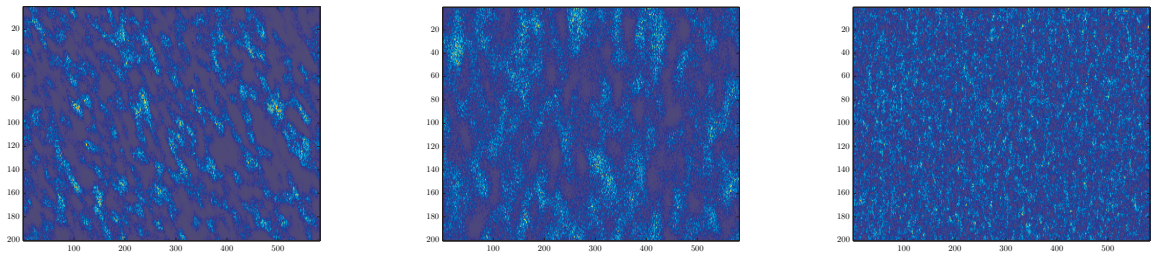

(a) $\nu = -0.5$ Rough (b) $\nu = 0.5$ Medium (c) $\nu = 2$ Sandy

Figure 3: Examples of Different Bottom Types for Different ν.

performs slightly better than the Rayleigh detector and this is due to a greater separation of the variances under the two hypotheses than the separation of the shape parameter for the Rayleigh assumption.

5.2 Performance Under Different Clutter Density and Coarseness

Another study was conducted on the effect of shape parameter (ν) on the detection performance. Using the calculated log-likelihood values another set of ROC curves were generated for each ν in the dataset, specifically for $\nu = -0.5$, $\nu = 0.5$, and $\nu = 2$ and the SNR was fixed at 12 dB. Lower values of ν correspond to rocky or rough textures while higher values of ν correspond to smooth sandy bottoms (see Figure 3). Figure 4a presents the ROC curves for the $\mathcal{K}$-distribution detector for each of the ν values with the P_D at the knee point for each curve indicated by a *.

Figures 4b and 4c give ROC curves generated using the same procedure described in the previous section. For all the ν values the $\mathcal{K}$-distributed detector has a much higher P_D (and lower P_{FA}) over the other detectors due to the fact that the overall distribution of the data is well-represented. The performance decreases as ν decreases for the $\mathcal{K}$-distributed detector as it becomes harder to accurately estimate the parameters of the distribution as the shape of the distribution gets narrower. Moreover, as the ν decreases the clutter becomes more dense making it harder for any of the detectors to distinguish between clutter and target.

For all the ν values the $\mathcal{K}$-distributed detector produces a much higher P_D. It is also interesting to note that for all ν values the Rayleigh and Gaussian-based detectors have identical performance.

5.3 Performance as a Function of Target Type

Lastly, another study was conducted on the effect of target type versus detection performance. Using the calculated log-likelihood values another set of ROC curves were generated for each of three target types in the dataset, cylinder, cone, and sphere with the SNR again being fixed at 12 dB. Figures 5a,b,c present the ROC curves for each of the target types for the $\mathcal{K}$-distribution detector, Rayleigh detector, and Gaussian detector, respectively. For the all target types the $\mathcal{K}$-distributed detector has a much higher performance over the other detectors. Moreover, all three detectors perform well on the sphere, but there is a decrease for the cone and the cylinder. It can be noted that the $\mathcal{K}$-distributed detector has a higher P_D for a lower P_{FA} compared to the other detectors for all of the target types due to the ability to accurately separate out the clutter from the target.

Overall, the $\mathcal{K}$-distributed detector provides promise in improving detection rates for detecting objects from sonar imagery.

6. CONCLUSION

In this paper, we developed a $\mathcal{K}$-distributed detector for the detection of objects in sonar imagery that exhibits $\mathcal{K}$-distributed background. This is motivated by the recent studies which reveal that the $\mathcal{K}$-distribution provides a good fit to background clutter in sonar imagery data. It has been shown that by using an approximation to the Bessel function we can formulate an explicit concise log-likelihood function for the $\mathcal{K}$-distributed random

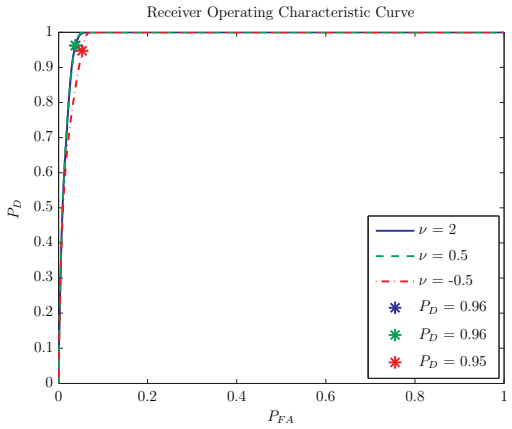

(a) K-Distribution

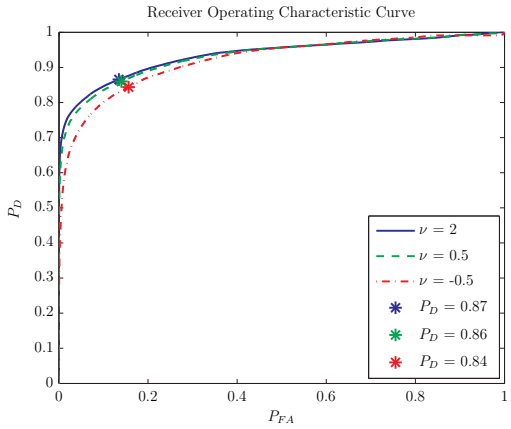

(b) Rayleigh Distribution

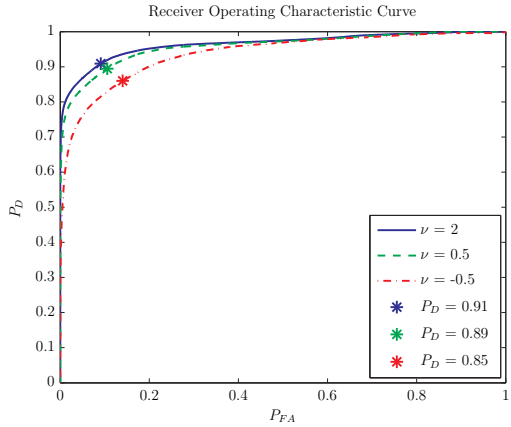

(c) Gaussian Distribution

Figure 4: Receiver Operating Characteristic Curves for Different Statistical Distribution Assumptions for Different ν.

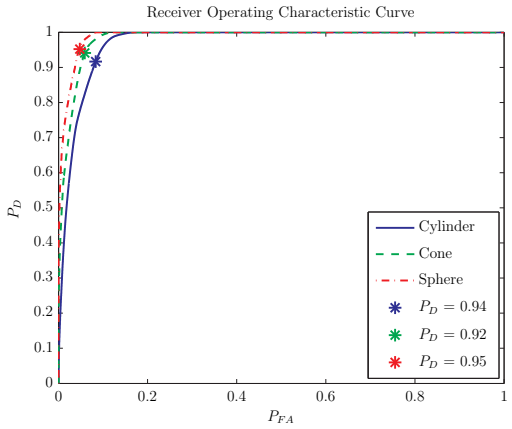

(a) K-Distribution

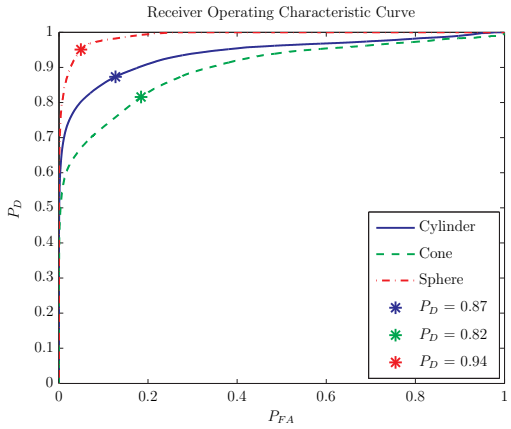

(b) Rayleigh Distribution

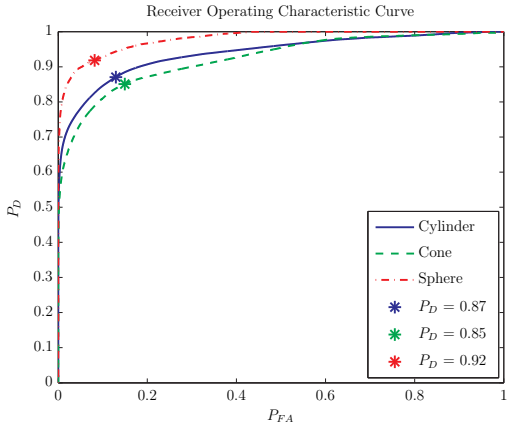

(c) Gaussian Distribution

Figure 5: Receiver Operating Characteristic Curves for Different Statistical Distribution Assumptions for Different Target Types.

variables. Our experiments on the synthetic sonar image data set provided by the NSWC PCD demonstrated good detection performance across all SNR's and different clutter density and coarseness of the $\mathcal{K}$-distributed detector over those of the Rayleigh and Gaussian-based detector. Overall, the $\mathcal{K}$-distributed detector shows promise in improving the detection rate while lowering the false alarm rate in the detection of underwater objects from sonar imagery data.

ACKNOWLEDGMENTS

This work was supported by the NSWC PCD In-house Laboratory Independent Research program funded by the Office of Naval Research. The authors would also like to thank J. Tory Cobb at NSWC PCD for providing the code to generate the sonar image backgrounds and technical support.

REFERENCES

1. G. J. Dobeck, "Fusing sonar images for mine detection and classification," *Proc. SPIE* **3710**, pp. 602–614, April 1999.
2. G. J. Dobeck, "Image normalization using the serpentine forward-backward filter: application to high-resolution sonar imagery and its impact on mine detection and classification," *Proc. SPIE* **5734**, pp. 90–110, April 2005.
3. C. Ciany and W. Zurawski, "Impact of image normalization and quantization on the performance of sonar computer-aided detection/computer-aided classification (CAD/CAC) algorithms," *Proc SPIE* **6553**, pp. 1T–9T, 2007.
4. T. Aridgides and M. F. Fernandez, "Automatic target recognition algorithm for high resolution multi-band sonar imagery," *Proc. of MTS/IEEE Oceans 2008 Conference* , pp. 1–7, Sep. 2008.
5. J. D. Tucker, M. R. Azimi-Sadjadi, and G. J. Dobeck, "Canonical coordinates for detection and classification of underwater objects from sonar imagery," *Proc. of IEEE OCEANS 2007 Conference Europe* , pp. 1–6, June 2007.
6. J. D. Tucker, N. Klausner, and M. R. Azimi-Sadjadi, "Target detection in m-disparate sonar platforms using multichannel hypothesis testing," *Proc. of MTS/IEEE Oceans 2008 Conference* , pp. 1–7, Sep. 2008.
7. T. Aridgides and M. Fernandez, "Enhanced ATR algorithm for high resolution multi-band sonar imagery," *Proc. SPIE* **6953**, pp. 0–1, March 2008.
8. T. Aridgides, P. Libera, M. Fernandez, and G. J. Dobeck, "Adaptive filter/feature orthogonalization processing string for optimal LLRT mine classification in side-scan sonar imagery," *Proc. SPIE* **2765**, pp. 110–121, April 1996.
9. S. Stanic and E. Kennedy, "Reverberation fluctuation from a smooth seafloor," *IEEE Journal of Oceanic Engr.* **18**, pp. 95–99, 1993.
10. S. Stanic, R. Goodman, K. Briggs, N. P. Chotiros, and E. Kennedy, "Shallow-water bottom reverberation measurements," *IEEE Journal of Oceanic Engr.* **23**, pp. 203–210, 1998.
11. J. T. Cobb and K. C. Slatton, "A parameterized statistical sonar image texture model," *Proc. SPIE* **6953**, pp. K1–K12, 2008.
12. J. T. Cobb, K. C. Slatton, and G. J. Dobeck, "A parametric model for characterizing seabed textures in synthetic aperture sonar images," *IEEE Journal of Oceanic Engineering* , to be published.
13. H. L. Van Trees, *Detection, Estimation, and Modulation Theory Part I*, John Wiley and Sons, 1968.
14. K. Ward, C. Baker, and S. Watts, "Maritime surveillance radar part 1: radar scattering from the ocean surface," *IEE Proc. Radar, Sonar Navig.* **137**, April 1990.
15. I. Gradshteyn and I. Ryzhik, *Table of Integrals, Series, and Products*, Academic Press, 1965.
16. E. Jakeman and P. Pusey, "A model for non-Rayleigh sea echo," *IEEE Trans. on Antennas and Propagation* **AP-24**, pp. 806–814, November 1976.
17. D. Abraham and A. Lyons, "Novel physical interpretations of K-Distributed reverberation," *IEEE Journal of Oceanic Engineering* **27**, pp. 800–813, October 2002.
18. E. L. Lehman, *Testing Statistical Hypotheses*, New York: Wiley, 1986.
19. P. Kasperkovitz, "Asymptotic approximations for modified Bessel functions," *Journal of Math Physics* **21**, pp. 6–13, January 1980.